Motor usage imprints microtubule stability in the shaft

Mireia Andreu-Carbó[1], Simon Fernandes[1], Marie-Claire Velluz[1], Karsten Kruse[1,2,3], Charlotte Aumeier[1,2]*

[1]Department of Biochemistry, University of Geneva, 1211 Geneva, Switzerland
[2]National Center for Competence in Research Chemical Biology, University of Geneva, 1211 Geneva Switzerland
[3] Department of Theoretical Physics, University of Geneva, 1211 Geneva Switzerland

*Correspondence to: Charlotte.aumeier@unige.ch

SUMMARY

Tubulin dimers assemble into dynamic microtubules which are used by molecular motors as tracks for intracellular transport. Organization and dynamics of the microtubule network is commonly thought to be regulated at the polymer ends, where tubulin-dimers can be added or removed. Here we show that molecular motors running on microtubules cause exchange of dimers along the shaft. These sites of dimer exchange act as rescue sites where depolymerising microtubules stop shrinking and start re-growing. Consequently, the average length of microtubules increases depending on how frequently they are used as motor tracks. An increase of motor activity densifies the cellular microtubule network and enhances cell polarity. Running motors leave marks in the shaft serving as traces of microtubule usage to organize the polarity landscape of the cell.

Keywords: Microtubule, kinesin, dynamics, in vitro, rescue, cell polarity

INTRODUCTION

Kinesins transport cargo (Verhey et al., 2011) and can also affect microtubule dynamics (Drummond, 2011). Microtubules are 25 nm wide tubes, polymerising at the tip by addition of α−β GTP-tubulin heterodimers. After incorporation at the plus-tip, GTP-tubulin dimers are hydrolysed (Mitchison & Kirschner, 1984). If GDP-tubulin dominates at the tip, then the microtubule experiences a catastrophe, they switch from a growing to a shrinking phase. While shrinking, tubulin dimers are removed from the plus-end. Recent reports showed that not only the tip, but also the rest of the microtubule, its 'shaft', shows a dynamic behaviour (Aumeier et al., 2016; de Forges et al., 2016; Dimitrov et al., 2008; Reid et al., 2017; Schaedel et al., 2015, 2019; Vemu et al., 2018). Tubulin can dissociate from the shaft spontaneously (Schaedel et al., 2019), or upon mechanical stress (Schaedel et al., 2015), resulting in damage sites along the GDP-shaft. These damage sites get repaired by incorporating GTP-tubulin. Some proteins have recently been reported to cause tubulin dissociation from the shaft or to mediate GTP-tubulin incorporation (Vemu et al., 2018; Triclin et al., 2018; Aher et al., 2020;). At a GTP-tubulin incorporation site, depolymerizing microtubules can be rescued and start re-growing. Therefore, sites of microtubule damage and dimer exchange are constructive areas leading to an increased microtubule lifetime (Aumeier et al., 2016).

By acting at the plus-end, kinesins can change the catastrophe rate (Arellano-Santoyo et al., 2017; Walczak et al., 1996) as well as the polymerisation (Hibbel et al., 2015; Howard & Hyman, 2003, 2007) and depolymerisation speeds (Arellano-Santoyo et al., 2017; Howard &

Hyman, 2003, 2007; Hunter et al., 2003), but no effect on the rescue rate has been previously reported *in vitro*. Binding of kinesin-1 to the microtubule shaft can change the microtubule conformation. Microtubules crowed with at least 10 % kinesin-1 show increased axial spacing between GDP-tubulin subunits, which resembles the elongated structure of a GTP-microtubule without changing the nucleotide state (Muto et al., 2005; Peet et al., 2018; Shima et al., 2018). Once bound to a microtubule, a kinesin-1 molecule runs across hundreds of tubulin dimers without dissociating (Block et al., 1990; Hancock & Howard, 1998). In a cell, kinesin-1 transports various cargos by binding preferentially to the subpopulation of microtubules that are acetylated and/or detyrosinated (Cai et al., 2009). These post-translational modifications have been proposed as underlying mechanisms for preferential binding (Cai et al., 2009; Hammond et al., 2010), but *in vitro* experiments showed only slight effects on the affinity of kinesin-1 for tubulin with posttranslational modifications (Kaul et al., 2014; Soppina et al., 2012).

While the role of microtubule tip-regulation is well established (Mitchison & Kirschner, 1984), regulation of the shaft in cells is largely unexplored. We previously showed that a local increase in shaft dynamics ultimately causes directed migration towards the site of the cell where shafts dynamics is increased and thereby the microtubule lifetime is prolonged (Aumeier et al., 2016).

Here we report how kinesin-1 activity regulates the lifetime and length of its microtubule-track by increasing shaft dynamics. We recently reported in a non-dynamic assay that the minus-end directed motor Klp2 causes tubulin dissociation from end-stabilised microtubules, and that this destabilise mechanically the microtubules in vitro unless tubulin incorporation is allowed (Triclin et al., 2018). Beyond an effect on the mechanic stability of microtubules in a static system, we show here by using dynamic *in vitro* assays and cells that kinesin-1 running on microtubules control microtubule network dynamics through rescue in the shaft. The increase in shaft dynamics is causing more rescue events, which result in a closer proximity between microtubule tips and the plasma membrane. We show that the effect of kinesin-1 on microtubule shaft dynamics ultimately results in a network asymmetry increasing the peripheral microtubule network.

RESULTS

Kinesin-1 induces tubulin incorporation along the microtubule shaft in a concentration dependent manner

To test whether running kinesins could induce tubulin-incorporation along the microtubule in a concentration dependent manner, we purified kinesin-1-GFP and performed an assay to monitor microtubule repair (Figure S1A). In our previously reported two-colour assay (Aumeier et al., 2016), we polymerised microtubules from green Atto488-tubulin dimers and stabilized the tip; then, for 15 minutes, we added free red Atto565-tubulin dimers which can continue to polymerise at the tip or get incorporated along the shaft. This allows us to monitor the incorporation sites, which appear along the shaft as red spots embedded in otherwise green microtubules (Figure 1A, and for important details and controls of this assay see Figure S1A).

While running on microtubules, kinesin-1 affected GTP-tubulin incorporation into the shaft. In the absence of kinesin-1, spontaneous tubulin incorporation sites covered only 4 % of the microtubules after 15 minutes (Figure 1B). Upon 15 minutes incubation with 5 nM running

kinesin-1, microtubule renewal was strongly enhanced: tubulin incorporation sites now covered 20% of the microtubules (Figure 1B). This increase is mainly due to a three-fold increase of the density of incorporation sites along the shaft (Figure 1C). Whereas the density of incorporation sites increased in the presence of running kinesin-1 in a concentration dependent manner (Figures 1C and S1B), the length of individual sites increased only slightly with the motor concentration (Figure 1D). This indicates that kinesin-1 caused defects in the microtubule shaft which were repaired by incorporation of GTP-tubulin dimers at a frequency that was considerably higher than the spontaneous frequency.

Running Kinesin-1 increase microtubule rescue frequency

Incorporation sites at the shaft have the potential to behave as rescue sites (Aumeier et al., 2016; de Forges et al., 2016; Vemu et al., 2018). To address whether the kinesin-1-mediated incorporation sites affect microtubule rescue, we looked at microtubule dynamics in the presence of running kinesin-1 (Figures S1C and S1D). We grew microtubules from GMPCPP-stabilized microtubule seeds in presence of 8 µM tubulin and 41 mM KCl, which yielded dynamic microtubules with an average length of 3.4 ±2.3 µm (n=344 microtubules, Figure 2A). Typically, shrinking microtubules disassembled completely and only in one fourth of the cases (85/384) a rescue event was observed (Figure 2A). After addition of kinesin-1, the shrinking velocity and the catastrophe frequency were not affected, and also the growth velocity remained comparable to the control (Figure 2B-D). In contrast, the rescue frequency increased up to four-fold with increasing kinesin-1 concentration (Figure 2D). In the presence of 2 nM kinesin-1, more than half of the shrinking microtubules were rescued (188/309).

The kinesin-1-dependent rescue events can be due to more incorporation sites. Alternatively, crowding of the kinesin-1 can lead to increased axial spacing between GDP-tubulin subunits (Muto et al., 2005; Peet et al., 2018; Shima et al., 2018) and could thereby influence the rescue frequency by itself. Kinesin-1-induced conformation changes of the GDP-shaft happen only above a kinesin-1 concentration of 10% (molar ratio with respect to tubulin) (Shima et al., 2018). In our assay, however, rescue events increased already four-folds at a concentration of 0.025% kinesin-1 at which the axial spacing is not affected. Therefore, the increased rescue events due to running kinesin-1 correlated with an increase in incorporation site frequency rather than with increased inter-dimer spacing, consistent with previous observations showing that incorporation sites are rescue sites (Aumeier et al., 2016; de Forges et al., 2016; Vemu et al., 2018).

Increase in microtubule rescue only happens if kinesin-1 runs

In the presence of the non-hydrolysable ATP analogue AMP-PNP, kinesins did bind to microtubules, but did not run (Hancock & Howard, 1999). In these conditions, the unbinding rate was also reduced and microtubules became densely covered by the motors (Figure S1E). Immotile kinesin-1 covering microtubules did not change the microtubule catastrophe frequency or depolymerisation behaviour (Figures 2E and S1E, S1F and Video S1). In contrast to the conditions in which kinesin-1 was motile, the rescue frequency was not increased in the presence of immotile kinesin-1, indicating that kinesin-1 binding by itself cannot generate rescue sites. In fact, the dense coverage of microtubules by immotile motors led to a decrease in the rescue frequency (Figure 2E), consistent with the possibility that immotile kinesin-1 could protect the shaft from spontaneous tubulin exchange. Therefore, only running kinesin-1 cause rescue sites.

Single Kinesin-1 runs can cause rescue events

To study the effect of single kinesin runs on the microtubule rescue frequency, we used 0.4 nM kinesin-1, a concentration which generates isolated, non-colliding runs on microtubules (Figure 2F). Under these conditions, the microtubule rescue frequency was already increased 1.5-fold with respect to controls without kinesin-1 (Figure 2D). At higher kinesin-1 concentrations, the rescue frequency increased linearly with the motor concentration showing that the effect of more kinesins was merely additive. Cooperative effects between kinesin-1 molecules were therefore unlikely to affect the rate of rescue. We conclude that tubulin incorporation along the microtubule can be triggered by single kinesin-1 molecules.

Kinesin-1 causes tubulin exchange rarely

How often does a single molecule of kinesin-1 lead to an incorporation site? After 15 minutes, the density of incorporation sites in the presence of 2 nM kinesin-1 was 0.14 ± 0.027 events/µm of which 0.06 ± 0.028 events/µm correspond to spontaneous events. Therefore, 2 nM kinesin-1 caused 0.08 incorporation-events per µm. Considering the number of motors binding to microtubules (5.2 kinesin-1/µm within 15 min), and the average kinesin-1 run length (1.4 ± 0.5 µm, Figure S1G), an incorporation site occurred every 91 µm along a kinesin-1-track. This implies that an incorporation site was induced every 11300 kinesin-1 steps. We conclude that kinesin-1 causes incorporation sites very rarely, but it seems that these rare events can change considerably the rescue frequency (Figure 2D).

To study if the rare tubulin incorporation events induced by running kinesins are in principle sufficient to explain our observed increased rescue frequencies, we performed stochastic simulations of the system. In the simulations, a microtubule is effectively described as a polymer represented by a dynamic linear lattice (Johann et al., 2012; Melbinger et al., 2012), with sites that are either in a 'GTP'- or 'GDP'-state (Video S2, Figure S2A, and see Methods). In sites where there is GTP, a rescue event can occur. We obtained the values for our simulation parameters from our *in vitro* experiments (Table S1). Only the probability at which a shrinking polymer rescues at a GTP-site could not be measured experimental and was therefore used as a fit parameter. The rescue frequency emerging from the simulations matched that observed experimentally in the absence of motor particles (Figures 2D and 2G).

To clarify the impact of kinesin-1 on tubulin incorporation along the shaft, we introduced motor particles in our simulation (Johann et al., 2012; Melbinger et al., 2012). Our data showed that motor particles moving on the lattice can change the state of individual lattice sites from GDP to GTP with a given probability p_X (Video S3, Figure S2B, and see Methods). For $p_X=1.8\times10^{-3}$, we reproduced in our simulations the kinesin-1-dependent rescue frequency observed experimentally. In our simulations, increasing the number of motor particles running on the polymer increased the rescue frequency in a concentration dependent manner, as we have observed experimentally (Figures 2D and 2G). Therefore, rare incorporations caused by running motors are still frequent enough to account for a considerable increase in rescue events as seen in our experiments.

Running kinesin-1 causes unlimited growth of microtubules

We noted in our simulations an increase in the average polymer length when motor particles were present (Figure 2G). The length increased with the number of motor particles moving on the lattice (Figure 3A and S2C). The density of motor particles on the polymer can be

adjusted by changing their binding rate in the simulation. We found that depending on the number of motor particles, the average polymer growth can be bound (i.e. reach a plateau) or unlimited (Figure 3A). In the simulations, at low motor particle density, the rescue frequency was low and growth was bound, because, following a catastrophe, many polymers depolymerised completely (70%). Thus, polymerisation and depolymerisation were balanced and a steady-state with constant average polymer length was reached. In contrast, at high motor particle density, which caused a high rescue frequency, complete depolymerisation could be observed only at initial stages of the simulation. In this scenario, frequent rescue events extended the polymer by adding length to a pre-existing lattice, leading to unlimited growth (Dogterom & Leibler, 1993). This unlimited growth regime occurred above a threshold value of motor particles which corresponded to the density observed experimentally at 2 nM kinesin-1.

In our *in vit*ro experiments, we assessed how the microtubule length depends on kinesin-1 concentration (Figure 3B). The microtubule length distribution was unimodal and the average value as well as the standard deviation increased over time (Figure 3C) (Jeune-Smith & Hess, 2010). The length distribution of microtubules was different with and without kinesin-1 and it depended on motor concentration as observed in the simulations. In the presence of 1nM kinesin-1, the average microtubule length increased and reached a plateau after 30 minutes (Figure 3D). In these conditions, the average length was larger than without motors (12.6 µm *versus* 5.8 µm after 30 min; Figure 3D). In contrast to the bound growth with 1nM kinesin-1, for 2 nM kinesin-1, the average microtubule length did not plateau: microtubules continued to grow. Above a critical kinesin-1 concentration, microtubule growth was unlimited, as observed in the simulations. Together, the *in vitro* and theoretical results show that kinesin-1-induced GTP-tubulin incorporation along the microtubule shaft increases dramatically the microtubule rescue frequency and average length. Above a critical concentration of running kinesin-1 on microtubules, the microtubule length distribution switches from a steady state regime to a behaviour of unlimited growth.

In cells, kinesin-1 activity promotes rescue events and controls microtubule lifetime

The results of our *in vitro* studies and numerical simulations indicated a positive feedback between the frequency at which microtubules are used as tracks by kinesins and the stability of those microtubules. We wondered whether this positive feedback changes the cellular organization of the microtubule network depending on kinesin activity. To address this question, we manipulated the concentration and activity of kinesin-1 in cells, and studied their effects on microtubule network dynamics, density and organization. To reduce the native kinesin-1 pool by 90 %, we performed a siRNA knockdown of kinesin-1 in CRISPR/Cas9 knock-in GFP-Tubulin Hela cells (Figure 4A). Lower concentration of kinesin-1 resulted in a 20% reduction of rescue frequency compared to control conditions (Figures 4B), in line with a previous observation (Daire et al., 2009). Therefore, kinesin-1 contributed considerably to the generation of rescue sites in the cellular microtubule network.

Conversely, we studied the effect of kinesin-1 activity on local microtubule shaft dynamics by using a kinesin-1 specific drug, Kinesore, in a Ptk2 cell line stably expressing GFP-Tubulin. Kinesore activates the native kinesin-1 pool by specifically interacting with the cargo binding site of kinesin-1 light chain (Randall et al., 2017). It thereby allows the binding and running of kinesin-1 on microtubules even in the absence of cargo upon addition of the compound.

Adding 100 µM Kinesore to Ptk2 cells increased the binding of kinesin-1 to microtubules by a factor of four (Figures 4C and S3A). As a consequence, the microtubule rescue frequency increased by 28% in Ptk2 cells (Figures 4D, 4E, and S3B). This higher rescue rate per microtubule led to a 1.5-fold increase of microtubule lifetime (Figure 4F). Increasing the activity of the cellular kinesin-1 pool resulted in higher microtubule shaft dynamics, higher rescue frequency and higher microtubule stability, similar to our observation *in vitro* at higher kinesin-1 concentrations (Figure 2D).

Control of rescue by kinesin-1 densifies the microtubule network and rearranges it in space

The kinesin-1 caused increase of microtubule lifetime influences the global microtubule network (Figure 5). We measured the GFP-Tubulin fluorescent intensity distribution in our Hela cells before and after Kinesore treatment. We segmented the pattern of GFP fluorescence intensity into three categories: low, intermediate and high. We calibrated the intensity in the categories so that they correspond to i) the intensity of cytoplasmic tubulin-dimers (low), ii) the intensity from single microtubules (in locations where individual microtubules can be distinguished; intermediate), and the intensity from higher density networks, where single microtubules cannot be resolved (high; Figure 5A and for details see S4A). Upon Kinesore incubation, the total tubulin-GFP fluorescence intensity associated to the high-density microtubule network increased at the expense of free tubulin-dimers and isolated single microtubules (Figures 5A, 5B, S4C, S4D and S5). We confirmed the effect of Kinesore treatment on the reduction of the abundance of cytoplasmic tubulin and on the increase of the microtubule network mass by Western blot (Figure S3C). This effect was specific for kinesin-1, since Kinesore treatment did not affect the microtubule network in kinesin-1 siRNA knockdown cells (Figure 5B).

The denser microtubule network after kinesin-1 activation was particularly apparent at the cell periphery (Figures 5C and S3D), where microtubules were sparse in Ptk2 control cells (Provance et al., 1993). Indeed, the average distance between the plasma membrane and the microtubule tip was reduced by half after 10 min of Kinesore treatment (Figure 5D). Furthermore, we also observed that the peripheral microtubule density increased upon expression of a constitutively active mutant of kinesin-1, kinesin-560, in Ptk2 cells (Figure S3E).

DISCUSSION

Taken together, our data show that kinesin-1 is not only using the microtubules as tracks for cargo delivery in cells, but, at the same time, it controls the length and lifetime of their preferred tracks. This is based on the following observations: i) running kinesin-1 increases microtubule rescue events (Figure 2D), ii) average length of microtubules increases depending on how frequently they are used as motor tracks (Figure 3), iii) active kinesin-1 densifies the cellular microtubule network and this enhances cell polarity. (Figure 4 and 5).

In the scenario where kinesin-1 controls microtubule stability by rescue, a positive feedback loop ensures that frequently used tracks become more stable. It is well established that kinesin-1 shows preferential binding to a subset of long-lived microtubules which are also acetylated and/or detyrosinated (Cai et al., 2009; Hammond et al., 2010). However *in vitro* experiments showed only slight effects on the affinity of kinesin-1 for tubulin with posttranslational modifications (Kaul et al., 2014; Soppina et al., 2012). It is therefore unclear

whether preferential binding to microtubules with these post-translational modifications is a cause or a consequence of these modification. Our observations are indicating that kinesin-1 controls the lifetime of a subset of microtubules which thereafter get post-translationally modified due to their increased lifetime.

Beyond the microtubule tips, including the microtubule shaft as a regulatory structure changes our understanding of the microtubule network from i) a spotted system which is only controlled in discrete points, at the end of filaments, to ii) a continuous system controlled and modified everywhere in the network. To support cell polarity, the microtubule network needs to be functionally and structurally asymmetric. The symmetry of a network array can be broken via four general mechanisms: relocation of existing microtubules within a cell; addition of an asymmetric nucleation site; repositioning of nucleation sites homogeneously distributed in the network to one side of a system; differential modulation of microtubule dynamics.

Kinesin-1 can break the network symmetry by differential modulation of microtubule dynamics. The preferential binding of kinesin-1 to a subset of microtubules within the network causes local stabilization and local increase in density of microtubules, which in turn increases kinesin-1 binding in that region. Indeed, this kinesin-1/microtubule positive feedback system can generate from minor heterogeneities in space, as an emerging property, a heterogeneous landscape of microtubules underlying cell polarity. Any slight spatial heterogeneity in the concentration of running kinesins will be then amplified. We did observe such amplifying heterogeneities upon cargo-independent activation of kinesin-1 (Figures 5E, 5F and S6). Therefore, the activity of the running motors can generate polarity inside the cell or amplify network heterogeneities encoded in other polarity cues (Par complex, planar cell polarity, directed migration, etc.).

These type of positive feedback loops could impact the generation of memory in the nervous system. When a neuron fires, demand of synaptic vesicle at the terminal implies trafficking along axonal microtubules, from the soma to the presynaptic site. Kinesin-mediated transport of synaptic vesicles along the axon could trigger the positive feedback loop we described here, reinforcing the trafficking of synaptic vesicles of those axonal tracks which have been frequently used and thereby contributing to the reinforcement of memory.

Acknowledgments: We thank O. Schaad for support with the statistical analysis, and M. Gonzalez-Gaitan for scientific discussions. S. Diez for sharing the Kinesin-1 plasmid and Kinesin purification experiences. M. Gonzalez, S. Hoogendoorn, P. Guichard, V. Hamel, and A. Roux for carefully reading of our manuscript. MAC and SF have been supported by the SNSF, 31003A_182473; KK has been supported by the NCCR Chemical Biology program; CA has been supported by the DIP of the Canton of Geneva, SNSF (31003A_182473), and the NCCR Chemical Biology program.

Author Contributions: MAC performed the experiments with the help of SF. MAC and CA designed the experiments. MCV purified the proteins and generated the CRISPR cell line. MAC, SF, MCV and CA analysed data. KK designed and performed numerical simulations. CA wrote the manuscript.

Declaration of Interests:

The authors declare no competing interests.

FIGURES

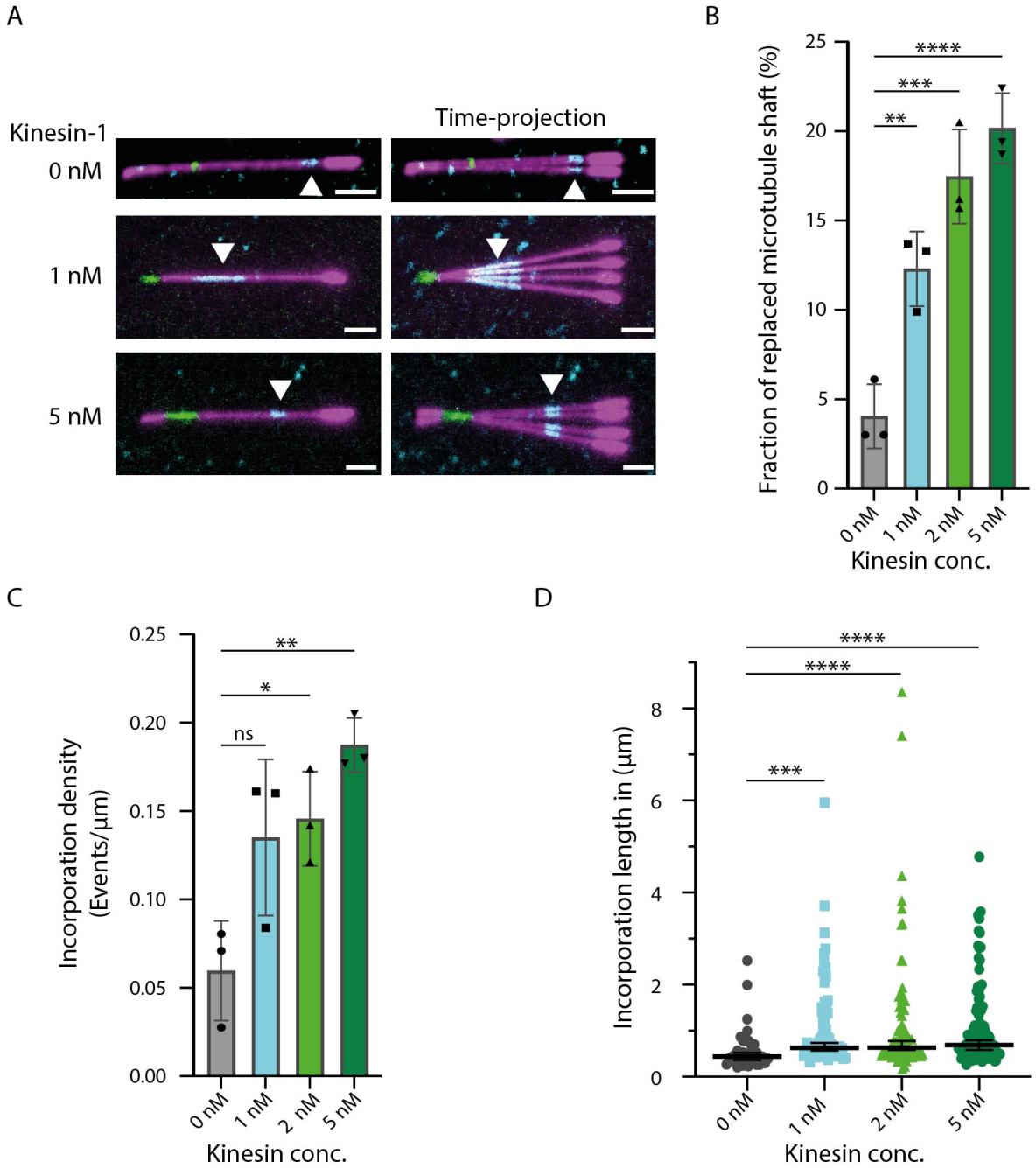

Figure 1. Kinesin-1 induces tubulin incorporation along the microtubule shaft.

(A) Tubulin incorporation sites (cyan) along GDP-microtubules (magenta; 20% labelled) grown from a seed (green) and capped by GMPCPP (magenta; 70% labelled) in presence of 0 nM, 1 nM, and 5 nM kinesin-1. White arrowheads: incorporation sites. Time projection (max intensity) of 4 subsequent images of single microtubules. Scale bar 2 µm.

(B) Fraction of replaced microtubule shaft (total length of all incorporation sites divided by the total microtubule length). Mean fraction in % with SD. Statistics: one-way ANOVA **P = 0.0066, ***P =0.0003, ****P < 0.0001.

(C) Density of incorporation sites (total number of incorporation sites divided by total microtubule length). Mean density with SD. Statistics: one-way ANOVA *P = 0.0345, **P =0.0039. For each condition in B and C, three independent experiments were analysed with a total of 128 (Control), 138 (1 nM kinesin-1), 135 (2 nM), 139 (5nM) microtubules.

(D) Length of incorporation sites. Median with 95% CI. For each condition, three independent experiments were analysed with a total of 37 (Control), 155 (1 nM kinesin-1), 143 (2 nM), and 201 (5 nM) incorporation sites. ***P=0.0001, ****P < 0.0001 with a Kruskla-Wallis test.

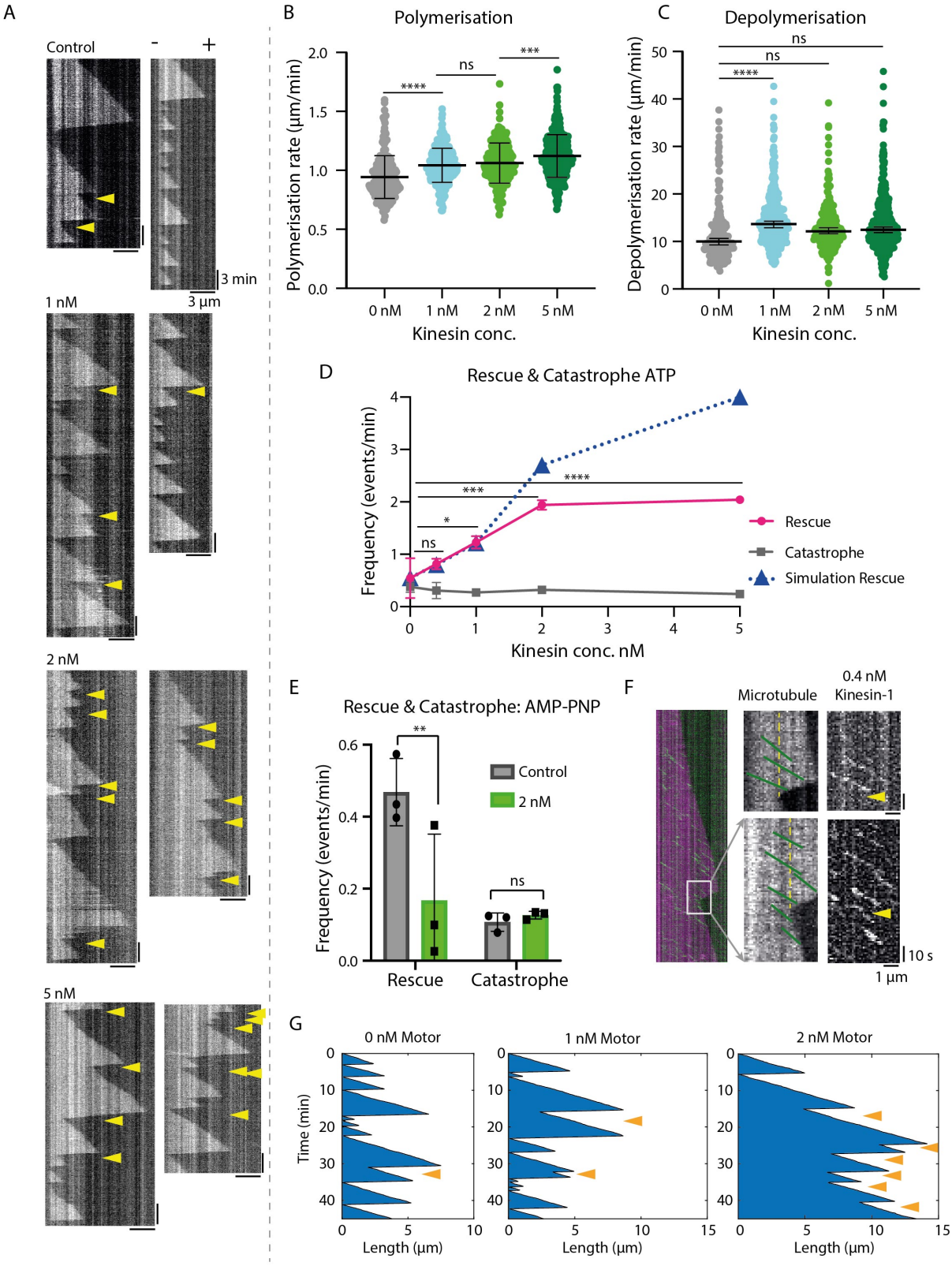

Figure 2. Running kinesin-1 increases microtubule rescue frequency.

(A) Representative kymographs of microtubule dynamics. Microtubules were polymerised from seeds in the presence of 8 µM tubulin and different kinesin-1 concentrations (0 nM, 1 nM, 2 nM, and 5 nM). Yellow arrowheads indicate rescue sites. Plus-ends are oriented to the right.

(B) Polymerisation speed of microtubules in presence of different kinesin-1 concentrations. ***P =0.0003, ****P < 0.0001 with a one-way ANOVA. Mean with SD.
(C) Depolymerisation speed of microtubules at different kinesin-1 concentrations. ****P < 0.0001 with two-way ANOVA with nested group in log transformed data. Median with 95% CI.
In B and C, the polymerisation and depolymerisation speeds were measured for three independent experiments with 296 (Control), 473 (1 nM kinesin-1), 307 (2 nM), and 528 (5 nM) microtubules in total.
(D) Rescue (pink) and catastrophe frequency (grey) as a function of kinesin-1 concentration. The rescue and catastrophe frequency were measured in 3-4 independent experiments for each condition with 389 (Control), 214 (0.4 nM kinesin-1), 661 (1 nM), 321 (2 nM), and 557 (5 nM) microtubules in total. *P = 0.0169, ***P =0.0001, ****P < 0.0001 with one-way ANOVA. Mean with SD. Blue: polymer rescue frequency at steady state obtained from simulations. Note that the experiments for 2 and 5 nM kinesin-1 had not yet reached steady state.
(E) Rescue frequency in the absence of kinesin-1 and in presence of immotile 2 nM kinesin-1 (1 mM AMP-PNP). The rescue and catastrophe events were measured in three independent experiments for each condition, total number of microtubules analysed: n=152 (Control); n=162 (2 nM kinesin-1). Mean with SD, multiple t test ns= 0.829, **P = 0.0076.
(F) Representative microtubule kymograph (8 µM tubulin, magenta, left) in the presence of running kinesin-1 (0.4 nM; green). In microtubule kymograph (middle) kinesin-1 tracks are drawn as green lines, future rescue site is indicated by yellow dashed line. Single kinesins show no change in walking behaviour at the future rescue site. Yellow arrowheads indicate rescue sites in kinesin kymograph (right).
(G) Numerical Simulations: Representative kymographs of polymer dynamics in presence of different motor particle attachment rates corresponding to different kinesin-1 concentrations in the experiments (0 nM, 1 nM, 2 nM). Orange arrowheads indicate rescue sites.

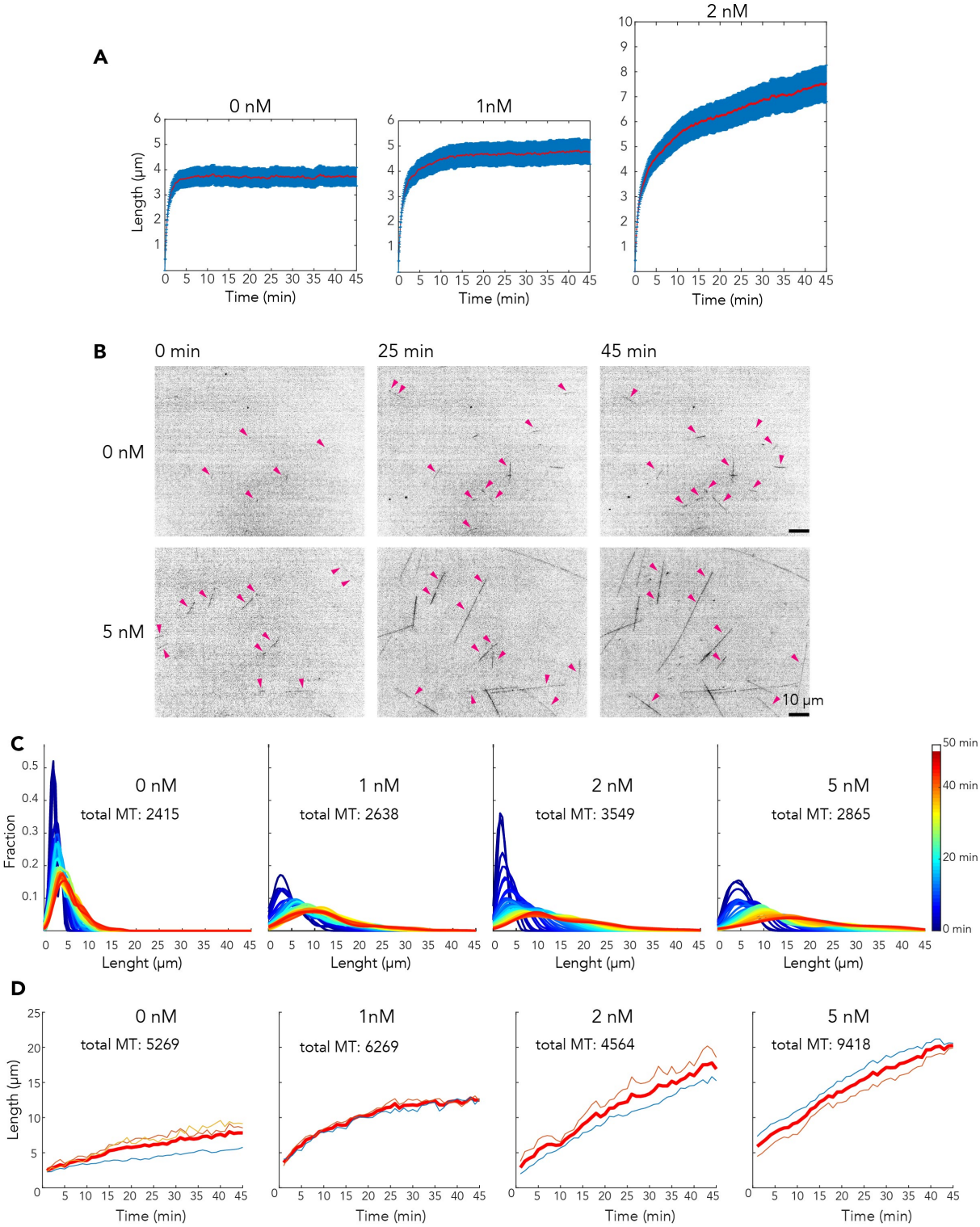

Figure 3. Kinesin-1 controls microtubule length.

(A) Numerical Simulations: Polymer length over time plotted for different motor particle concentrations: 0 nM (Control), 1 nM and 2 nM motor particles. Mean length (red) with SE (blue). Increasing the polymerisation rate of the polymer did not affect the median polymer length (Figure S2C).

(B) Images from a time lapse showing microtubules (8 µM tubulin) in presence of 0 nM or 5 nM kinesin-1 (imaging rate: 1/min, Video S4 and S5). Addition of kinesin-1 increased the net

polymer mass after 25 min in the field of view. The net polymer mass further increased after 45 min. Magenta arrows indicate microtubules which were measured for the statistics in Figures C and D (crossing microtubules and microtubule bundles were excluded from the statistics). Scale bar 10 µm.

(C) Microtubule length distribution over time (see LUT) at different kinesin-1 concentrations: 0 nM (Control), 1, 2 and 5 nM kinesin-1. Microtubules were imaged every minute for 45 min. To exclude rescue events influenced by bundling or crossing between microtubules, we excluded those events. Total number of microtubules analysed in each concentration condition is indicated. **(D)** Mean microtubule length over time of three independent experiments at different kinesin-1 concentrations: 0 nM (Control), 1, 2 and 5 nM kinesin-1. Microtubules were imaged every minute for 45 min. Thin coloured curves represent mean length of each of the individual experimental repeats. Red curves represent the mean length for the three repeats. Total microtubule numbers analysed are indicated.

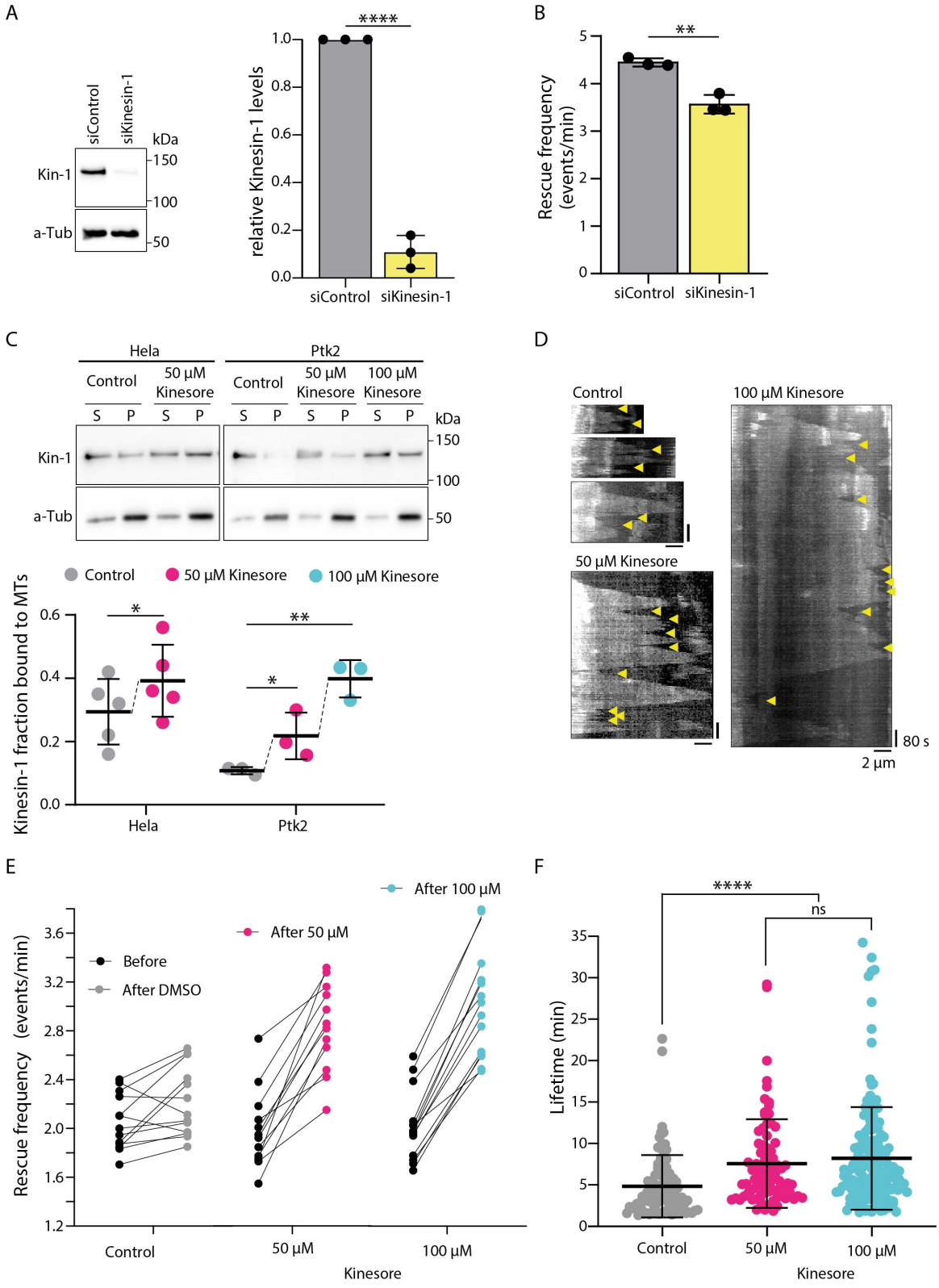

Figure 4. Kinesin-1 activity regulates microtubule dynamics and lifetime in cells.
(A) Representative Western Blot with quantification of kinesin-1 expression levels in kinesin-1 knockdown GFP-Tubulin Hela cells. Knockdown of kinesin-1 (siRNA kinesin-1) shows an 80-90% reduction compared to control cells (siRNA Control) from three independent experiments. ****, P<0.0001, two-tailed T test. Mean with SD.

(B) Kinesin-1 knockdown in GFP-Tubulin Hela cells (siRNA kinesin-1) decreases microtubule rescue frequency compared to control cells (siRNA Control). n=200 microtubules from 14 cells (siRNA Control) and n=180 microtubules from 12 cells (siRNA kinesin-1) from three independent experiments. **, P=0.0021, two-tailed T test. Mean with SD.
(C) Kinesore addition for 15 min increases kinesin-1 binding to microtubules (MT, Pellet fraction, P). Representative Western Blot with quantification. Fraction of active kinesin-1 bound to microtubules determined by the Kinesore-dependent microtubule binding assays for kinesin-1 (see methods). Control (0.1 %, or 0.2 % DMSO), 50 µM and 100 µM Kinesore treated Hela and Ptk2 cells. Mean with SD from three to four independent experiments. Relative binding values are shown in Figure S3A. Ptk2 *, P=0.0326, **, P=0.0051; Hela *, P=0.0453 unpaired T test.
(D) Representative kymographs of microtubules in GFP-Tubulin Ptk2 cells treated with 0.2 % DMSO, 50 µM Kinesore and 100 µM Kinesore. Yellow arrowheads indicate rescue events.
(E) Rescue frequency measured in GFP-Tubulin Ptk2 cells before and after treatment with 0.2% DMSO (Control), 50 µM Kinesore and 100 µM Kinesore. Each black circle (to the left) represents the rescue frequency of 10 microtubules in Ringer's buffer and it is connected to a grey, magenta or cyan circle (to the right) representing the rescue frequency of 10 microtubules after DMSO (n=13 cells), 50 µM (n=12 cells) or 100 µM Kinesore (n=14 cells) is added to the same cells. Fold change in rescue frequency is shown in Figure S3B.
(G) Microtubule lifetime after treatment with 0.2% DMSO (Control; n=90, from 9 cell), 50 µM Kinesore (n=80, from 8 cell) and 100 µM Kinesore (n=156, from 7 cells) in GFP-Tubulin Ptk2 cells from three independent experiments. ns, P=0.44; ***, P=0.0001; ****, P<0.0001, two-tailed T test. Mean with SD.

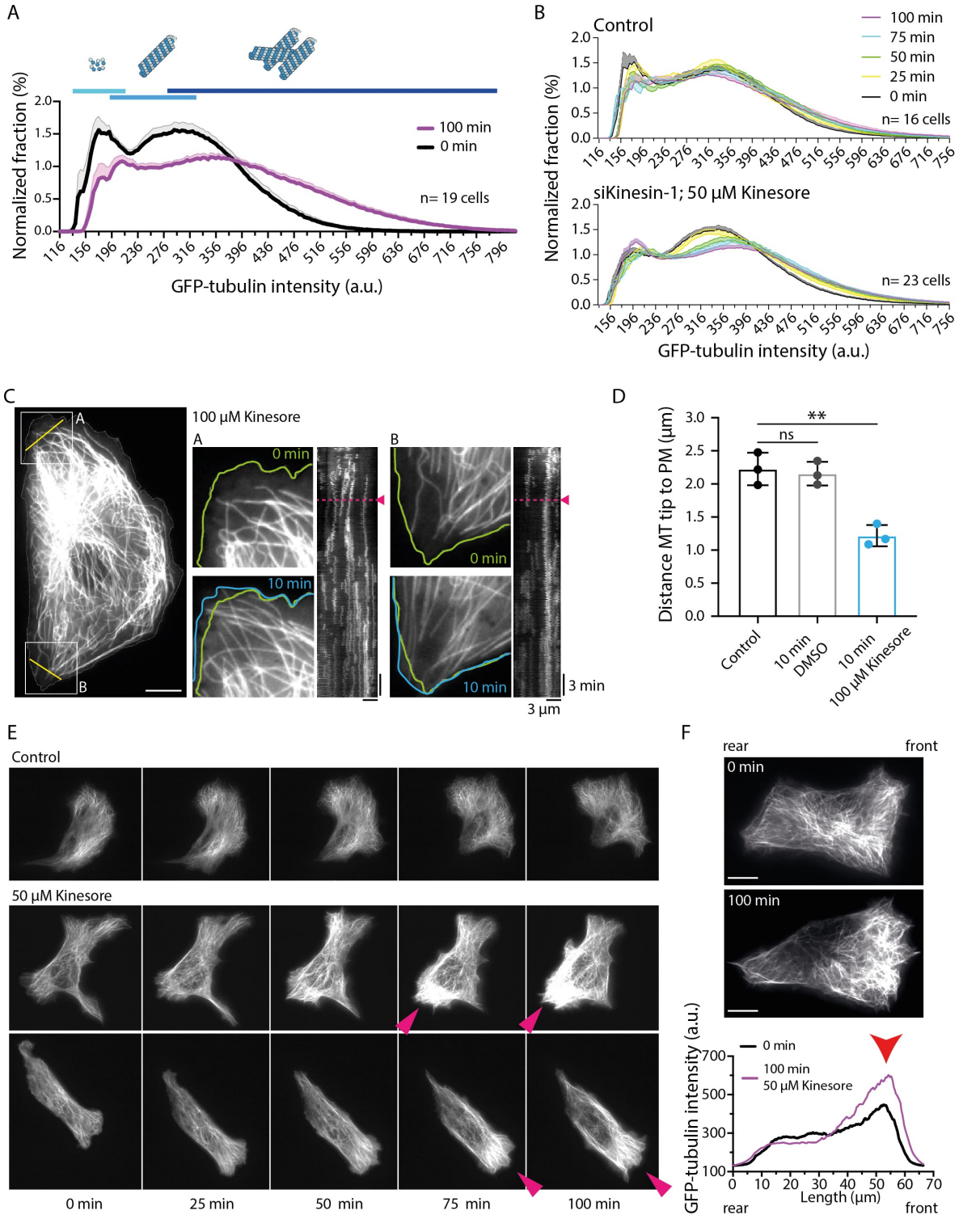

Figure 5. Kinesin-1 regulates microtubule network mass and organization in cells.
(A) Distribution of GFP-Tubulin fluorescent intensity before and after 100 min of 50 µM Kinesore treatment, measured in GFP-Tubulin Hela cells. Mean percentage of total fluorescent GFP-Tubulin intensity (n=19 cells); shaded area indicates SEM. Histograms of single cells are shown in Figure S5. Fluorescent intensity is grouped into three categories, cytosolic dimers (light blue), single microtubules (medium blue), and higher density network (dark blue). Kinesin-1 activation by Kinesore shifts the histogram to higher fluorescent

intensities indicating association of tubulin to dense networks of microtubules. For important control conditions see Figure S5A.

(B) Normalized fraction of the GFP-Tubulin fluorescent intensity in Hela cells. Cells were imaged every 5 min for 100 min after the addition of 0.1% DMSO to GFP-Tubulin Hela cells (Control), or 50 µM Kinesore to kinesin-1 knockdown GFP-Tubulin Hela cells. The increment of the microtubule network is kinesin-1 dependent. DMSO does not affect the microtubule mass and the histogram curve is not shifting higher fluorescent intensities. Normalized Mean with SEM. Further examples and corresponding Western blot of kinesin-1 expression levels in GFP-Tubulin Hela cells are shown in Figure S4.

(C) Representative GFP-Tubulin Ptk2 cell before and after 10 min of 100 µM Kinesore treatment. The zoom-in (white square) shows a representative microtubule network reorganization upon Kinesore treatment. Kymographs (from yellow lines) show an increase in microtubule number after 4 min of Kinesore addition (magenta arrowhead, dotted line). The effect is enhanced over time (Video S6). Further example shown in Figure S3D. Scale bar: 10 µm.

(D) Distance from the microtubule (MT) tips to the plasma membrane (PM) before treatment (Control), and after 10 min treatment with 0.2% DMSO, or 100 µM Kinesore. For each condition three independent experiments were performed: Control; n=90 MT from 12 cells, 0.2% DMSO; n=80MT from 12 cells, 100 µM Kinesore; n=156 MT from 12 cells). ns, P=0.71; **, P=0.0014, two-tailed T test. Mean with SD.

(E) GFP-Tubulin Hela cells imaged every 5 min for 100 min after incubation with 0.1 %DMSO (Control) or 50 µM Kinesore. The microtubule network organization is not affected by DMSO addition. Addition of Kinesore leads to reorganization of the microtubule network towards the cell rear. The network density increases (magenta arrowheads) where pre-established polarity occurred. Further examples are shown in Figure S6.

(F) GFP-Tubulin Hela cell before and after 100 min incubation with 50 µM Kinesore (top). GFP-Tubulin fluorescence intensity along line scans (bottom). A pre-existing heterogeneity in density of the microtubule network is amplified by Kinesore treatment (red arrow). Scale Bar 10 µm.

Supplementary Information:

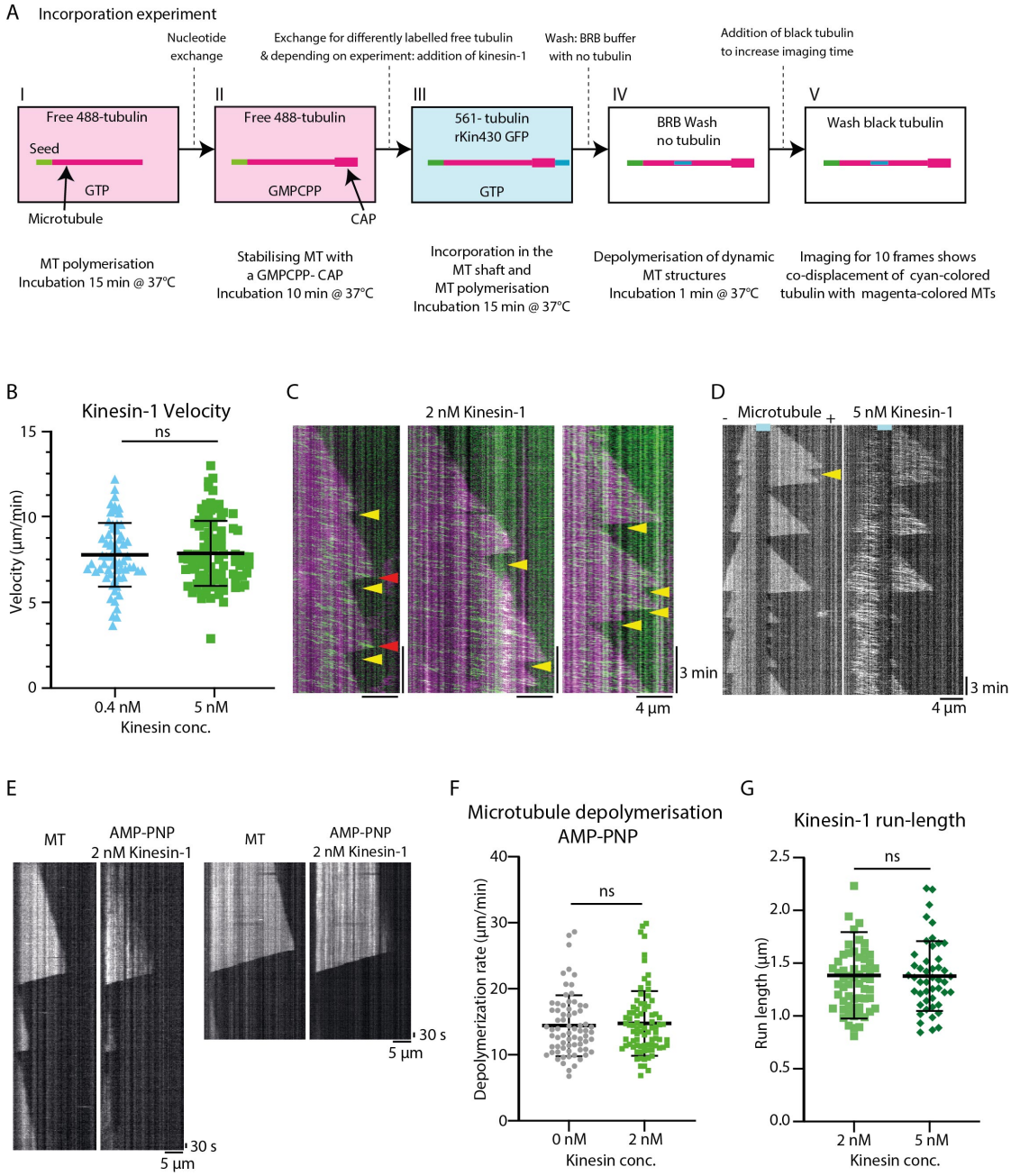

Figure S1. Incorporation Assay and microtubule dynamics in the presence of kinesin-1.
(A) Experimental setup of the incorporation assay . Flow chamber enables sequential exchange of solutions. **I** Microtubules polymerise form GMPCPP-seeds in the presence of tubulin 8 µM (20 % labelled), **II** Stabilizing GDP-microtubules with a GMPCPP-Cap. Exchange of nucleotide from GTP to GMPCPP and free tubulin 5 µM (70 % labelled), **III** Incorporation condition with 9 µM tubulin (100% labelled different colour) and kinesin-1 at different concentrations (0 nM, 1 nM, 2 nM, or 5 nM), **IV** Depolymerisation of all dynamic structures grown on top of the microtubule **in** BRB with no tubulin, **V** Stabilizing the microtubule for imaging with 8 µM black tubulin.
(B) Kinesin-1 added to the incorporation assay moved along microtubules at an average velocity of 7.7 µm/min, comparable to published data (Furuta et al., 2013). Mean with SD of

two independent experiments with a total of analysed kinesin-1 tracks: n=106 (0.4 nM), n=161 (5 nM); unpaired T test ns=0.7931.

(C) Representative kymographs of dynamic microtubules (8 µM tubulin, magenta) in presence of running kinesin-1 (2 nM, green). Yellow arrowheads indicate rescue sites. Red arrowheads indicate colliding of kinesin-1 which was not leading to rescue events or changing the microtubule depolymerisation behaviour.

(D) Representative kymograph of a dynamic microtubule (8 µM tubulin) and corresponding kymograph of running kinesin-1 (5 nM). Yellow arrow indicates rescue site. Only few kinesins were found on the Taxol stabilized GMPCPP-seed (cyan line). Plus- and minus-ends are indicated.

(E) Only running kinesin-1 induces microtubule rescue. Representative kymographs of dynamic microtubules (6.5 µM tubulin) and corresponding kymographs of immotile kinesin-1 (2 nM) in the presence of AMP-PNP. Immotile kinesin-1 densely covered the microtubule. Microtubule depolymerisation did not change in the presence of immotile kinesin.

(F) Microtubule depolymerisation rate (6.5 µM tubulin) in the presence of AMP-PNP and in absence or in presence of kinesin-1 (2 nM). Depolymerisation rates were measured in 3 independent experiments for each condition with a total of n=71 (0 nM), n=82 (2 nM) microtubules; ns, P=0.65; unpaired T test. Mean with SD.

(G) Kinesin-1 run length in the presence of 8 µM tubulin at different kinesin-1 concentrations. Kinesin-1 run lengths were measured in 2 independent experiments for each condition with a total of n=163 (2 nM), n=69 (5 nM) tracks; ns, P= 0.9328; unpaired T test. Mean with SD.

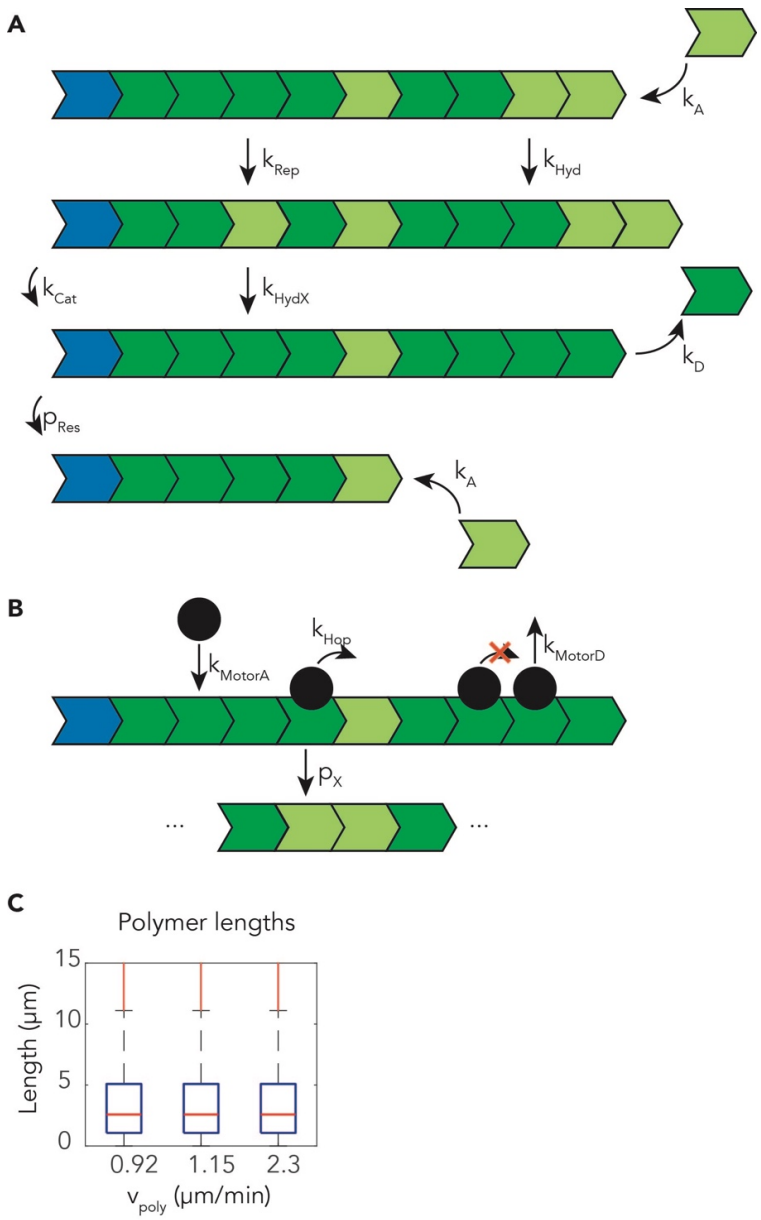

Figure S2.

(A) Illustration of polymer dynamics according to the different parameters encoded in the simulation. GTP- or GDP-tubulin dimer were encoded as lattice sites (light green for GTP-tubulin dimer and dark green for GDP-tubulin dimer). The polymer seed is represented in blue. Dynamical parameters are highlighted (for values see Methods, Table S1).

(B) Illustration of motor particles interacting with the polymer according to the different parameters encoded in the simulation. Motor particles are represented by black dots. Dynamical parameters are highlighted (for values see Methods, Table S1).

(C) Numerical Simulations: Polymer length at different polymerisation speeds observed experimentally (Figure 2B) in presence of different kinesin-1 concentrations (0.92 µm/min for 0 nM, and 1.15 µm/min for 5 nM). A scenario with double velocity (2.3 µm/min) was also considered. Note that the microtubule length is not affected by the polymerisation speed. Median (red line) with 25th and 75th percentiles (blue box) are indicated.

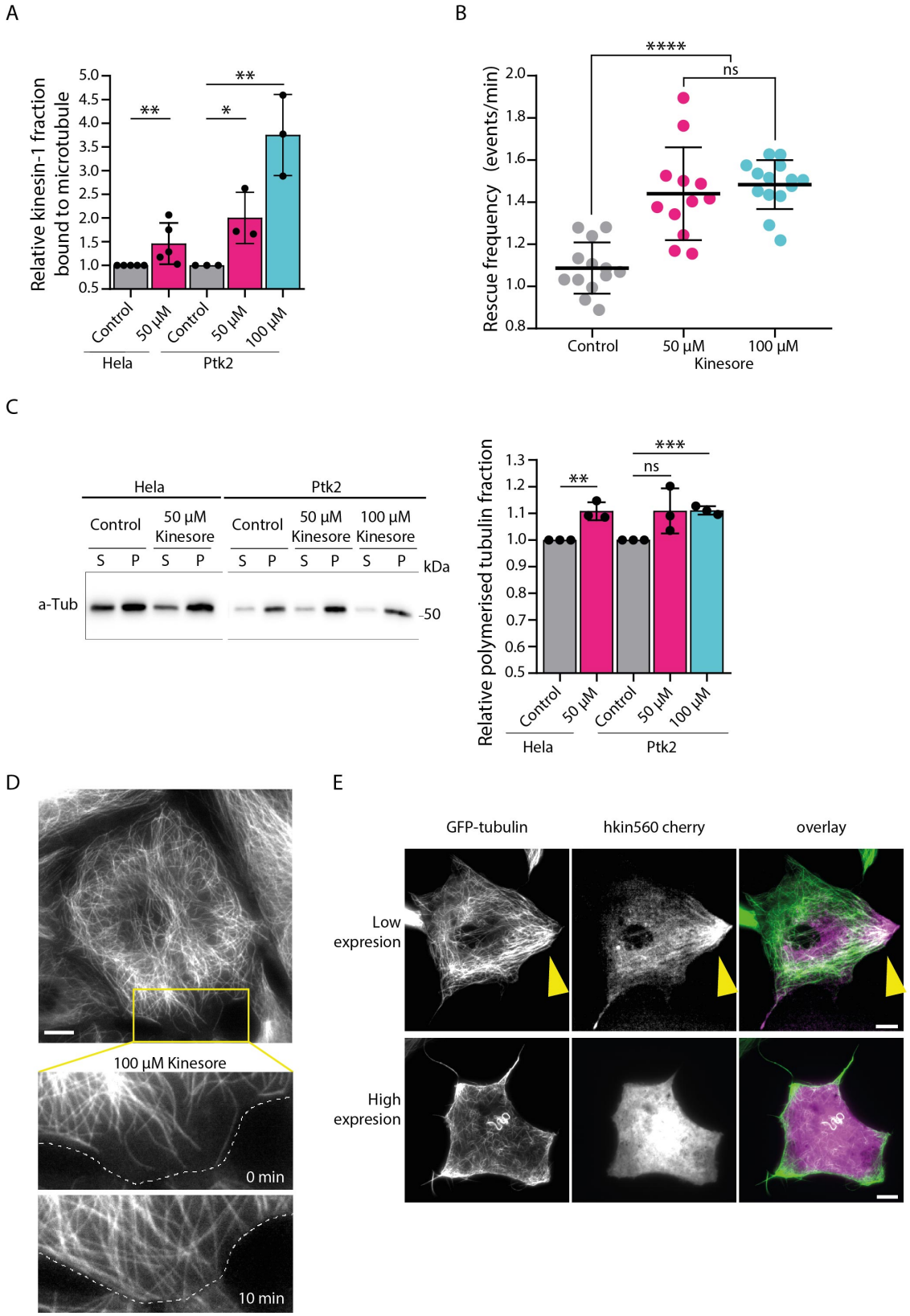

Figure S3. (A) Kinesore addition for 15 min increases kinesin-1 binding to microtubules. Relative binding of active kinesin-1 (bound to microtubules) after treatment with 0.1% or 0.2% DMSO (Control), 50 µM Kinesore, and 100 µM Kinesore in Hela and Ptk2 cells. Mean with SD from three to four independent experiments.

(B) Fold change of microtubule rescue frequency before and after Kinesore treatment in GFP-Tubulin Ptk2 cells. Cells were treated with 0.2% DMSO (Control; n=130 MT from 13 cells), 50 µM (n=120 MT, from 13 cell) and 100 µM Kinesore (n=140 MT from 14 cell) and the dynamics of single microtubules were analysed in three independent experiments. ****, P<0.0001, ns, P=0.53, two-tailed T test. Mean with SD.
(C) Effect of Kinesore on microtubule mass. Representative Western Blot with quantification. Hela cells were treated with 0.1% DMSO or 50 µM Kinesore, Ptk2 cells were treated with 0.2 % DMSO, 50 µM, and 100 µM Kinesore for 40 min at 37°C. Cells were lysed and microtubules (pellet fraction, P) were separated from the cytosolic tubulin dimer pool (supernatant fraction, S). The two fractions were analysed by Western blot. Mean relative tubulin levels present in the pellet with SD from three independent experiments. ns, P=0.0898, **P=0.0053, ***P=0.0002, unpaired T test.
(D) The zoom-in (yellow square) shows a representative microtubule network reorganization after 100 µM Kinesore treated GFP-Tubulin Ptk2 cells (Video S7). The cell outlines, indicated with white dashed lines, help to show that the microtubule tips are closer to the plasma membrane after 10 min of Kinesore addition.
(F) Representative TIRF images of GFP-Tubulin Ptk2 cells transfected with a constitutively active mutant of kinesin-1, hkinesin-560. In hkin560 low expression cells, local increase of microtubule density was observed. The yellow arrowhead indicates a region of microtubule network enrichment colocalizing with kinesin-1. In hkin560 high expression cells, the MT architecture was completely altered. Scale bar 10 µm.

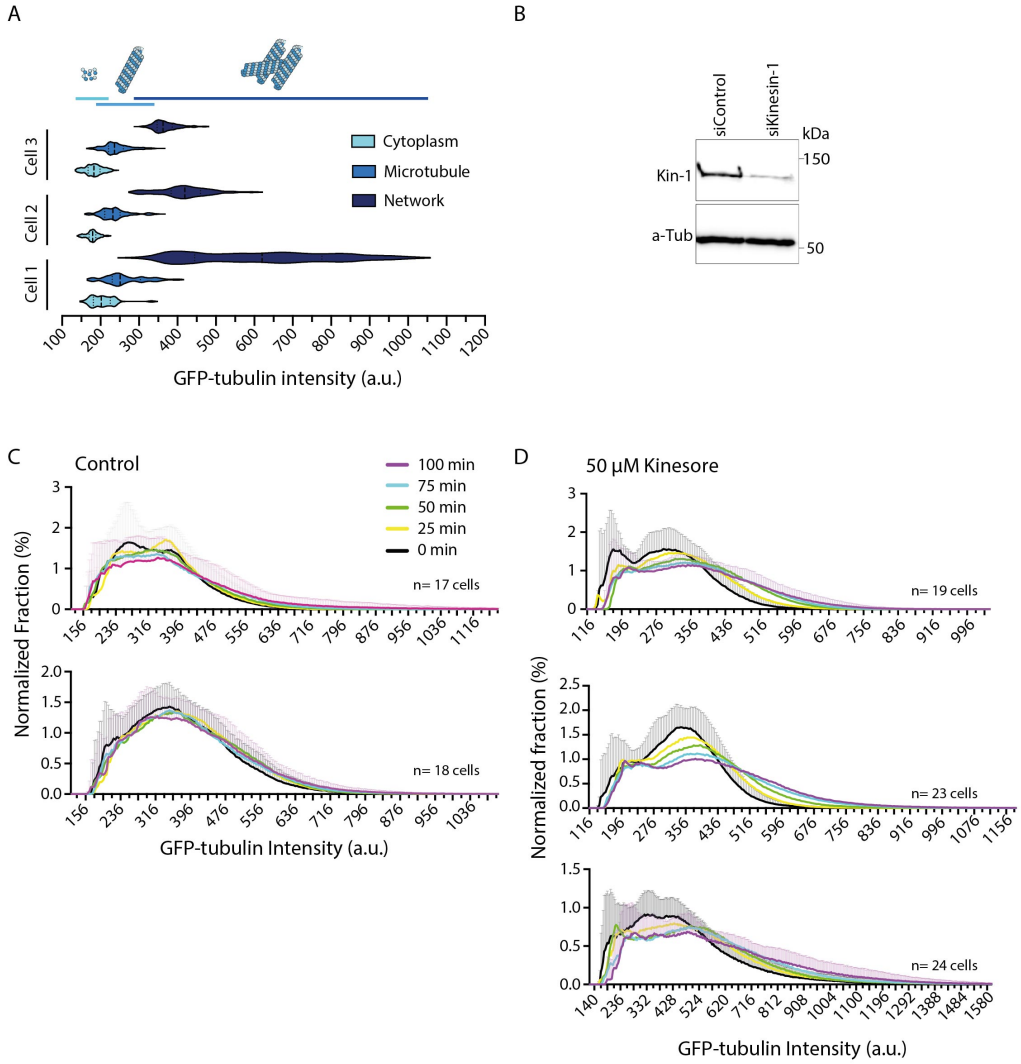

Figure S4. Kinesin-1 activity increases microtubule network and reduces free dimer pool.
(A) Subdivision of the GFP-Tubulin fluorescent intensity in Hela cells. Fluorescent intensity was measured at cytoplasm (tubulin dimers), along single microtubules, and in areas of denser microtubule network. Illustration above the graph shows the subdivision of fluorescent intensity into the three groups: tubulin dimer, single microtubules, microtubule network. Three cells from three independent experiments. Total measured grey values: cytoplasmic tubulin dimers (n=1504), single microtubule (n=2008), microtubule network (n=1608).
(B) Corresponding Western blot of kinesin-1 expression levels in GFP-Tubulin Hela cells knockdown for kinesin-1 (siRNA kinesin-1) used for fluorescent intensity analysis in Figure 5B. C and D shows mean normalized fraction of the GFP-Tubulin fluorescent intensity in Hela cells. Cells were imaged every 5 min for 100 min after the addition of 50 µM Kinesore or 0.1% DMSO (Control). Normalized Mean with SEM. Legend shown in C.
(C) DMSO is not affecting the microtubule mass and the histogram curve is not shifting higher fluorescent intensities over time. Three independent experiments (here and in Figure 5B) shown with a total of 51 analysed cells. The legend is shown on the right.
(D) Kinesin-1 activation through Kinesore shifts the histogram to higher fluorescent intensities over time. The microtubule mass is increasing and the free dimer pool decreasing. Three independent experiments shown with a total of 66 analysed cells.

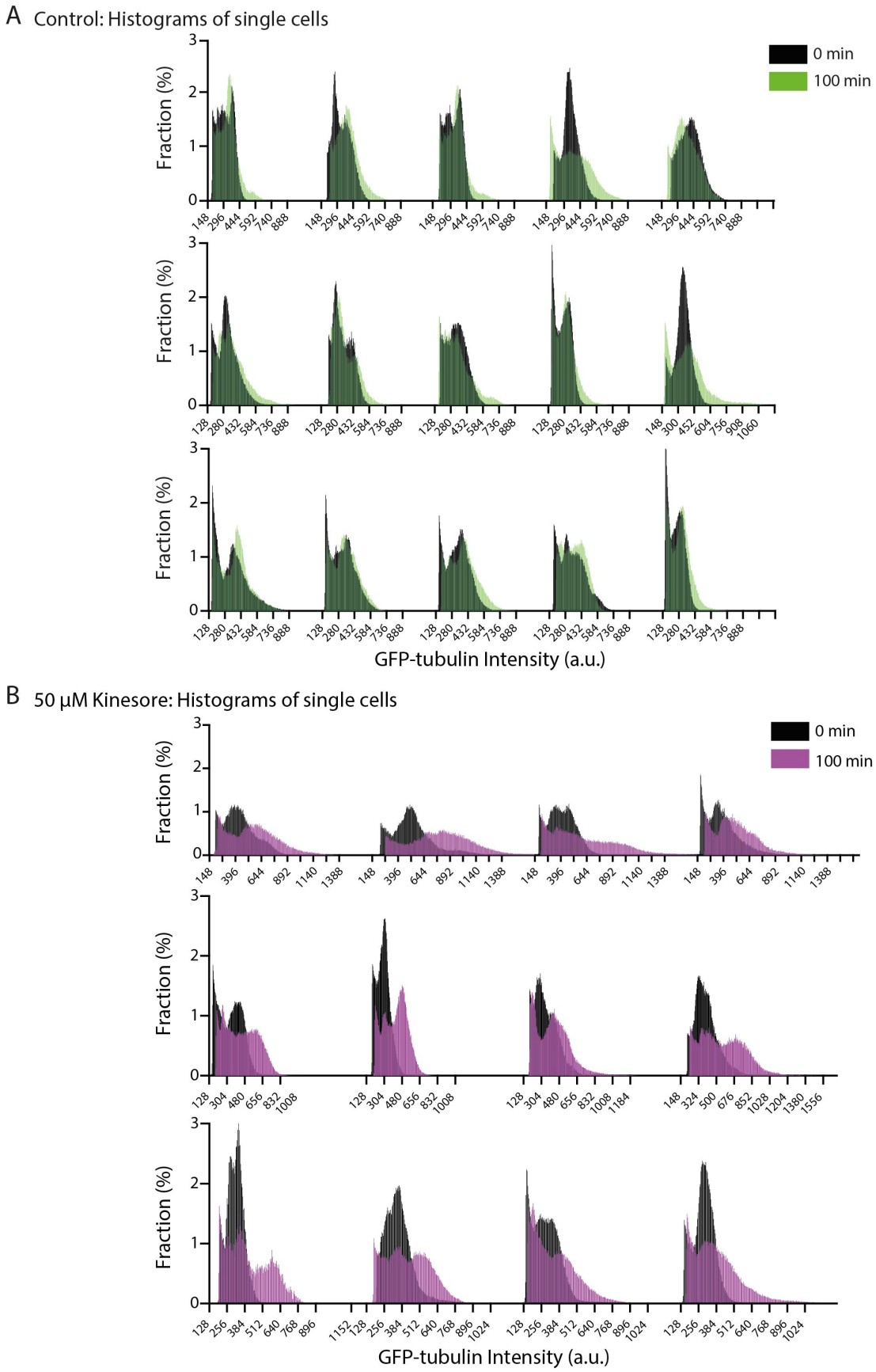

Figure S5. Kinesin-1 activity is increasing the microtubule mass in cells.

(A) Representative histograms of the GFP-Tubulin fluorescent intensity distribution of 15 single Hela cells from three independent experiments. Before (black) and after 100 min of addition of 0.1 % DMSO (green). DMSO is not increasing the microtubule mass.
(B) Representative histograms of the GFP-Tubulin fluorescent intensity distribution of 12 single Hela cells, from three independent experiments. Before (black) and after 100 min of addition of 50 µM Kinesore (magenta). The fluorescent intensity after Kinesore treatment is shifting towards higher values. The free tubulin dimer-pool is reduced and the microtubule network increased.

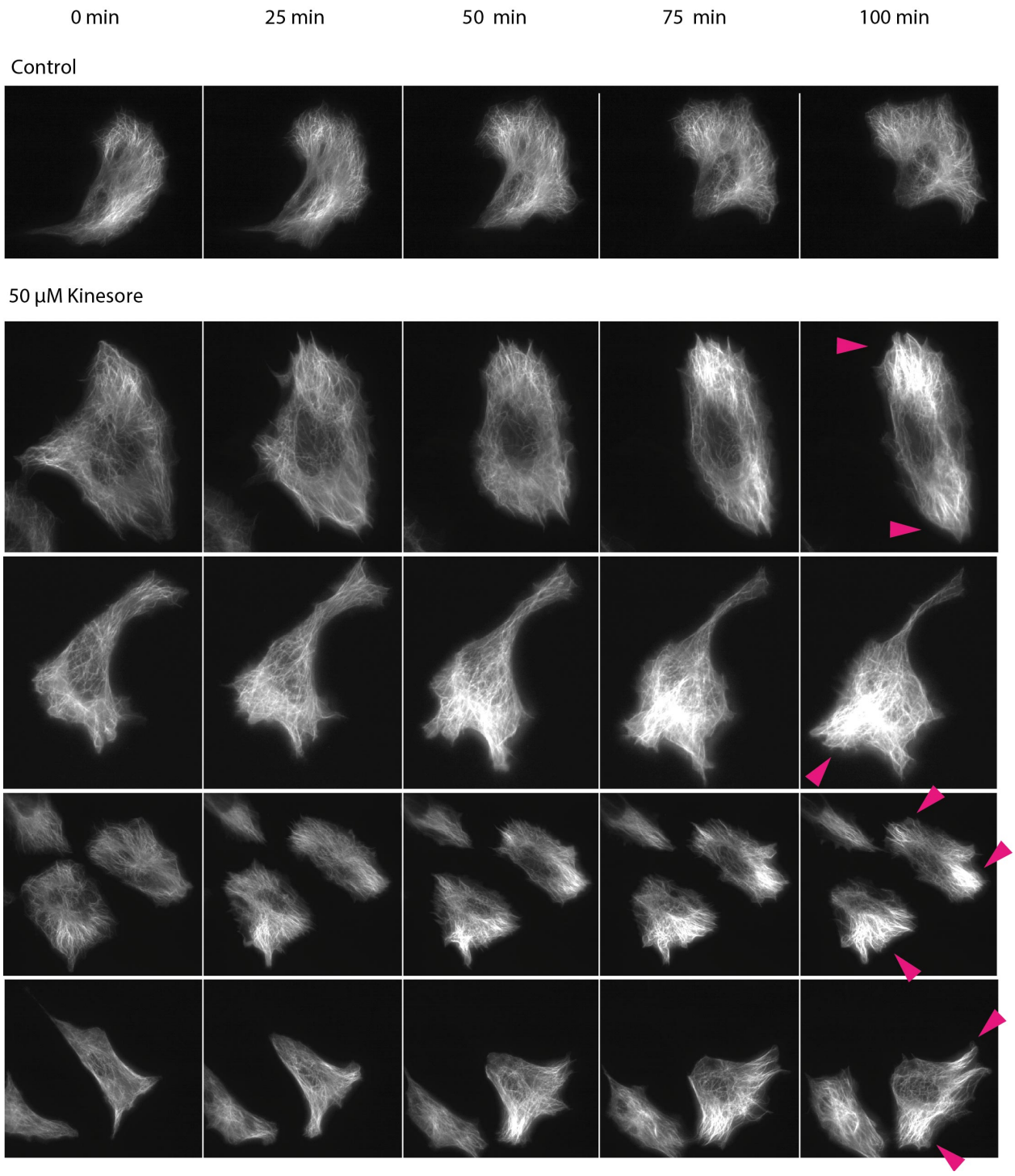

Figure S6. Kinesore affecting cell polarity. GFP-Tubulin Hela cells imaged every 5 min for 100 min after 0.1 %DMSO (Control) or 50 µM Kinesore addition. The microtubule network organization is not affected by DMSO addition. Addition of Kinesore leads to reorganization of the microtubule network towards the cell rear. The network density increases (magenta arrowheads) where pre-established polarity occurred.

Video S1.
Immotile kinesin-1 (2 nM, magenta) bound to dynamic microtubule (8 µM, green), does not change the microtubule depolymerisation behaviour.

Video S2.
Simulation of polymer dynamics in the absence of motor particles over 45 min. The seed is represented in blue. In the polymer the GDP-tubulin dimers are represented in dark green and the GTP-tubulin dimers in light green.

Video S3.
Simulations of polymer dynamics in the presence of 2 nM motor particles over 45 min. The seed is represented in blue. In the polymer the GDP-tubulin dimers are represented in dark green and the GTP-tubulin dimers in light green. Motor particles running along the polymer are represented in black.

Video S4.
Microtubule (8 µM tubulin) length in the absence of kinesin-1 over 45 min imaged every minute.

Video S5.
Microtubule (8 µM tubulin) length in the presence of 5 nM kinesin-1 over 45 min imaged every minute.

Video S6.
Microtubule network organization before and after 100 µM Kinesore incubation in GFP-Tubulin Ptk2 cells. Zoom-in of microtubules close to the plasma membrane. Distance between microtubule tips and plasma membrane is reducing after 10 min of Kinesore addition. The effect is enhanced over time.

Video S7.
Microtubule network organization before and after 100 µM Kinesore incubation in GFP-Tubulin Ptk2 cells. Zoom-in of microtubules close to the plasma membrane. Distance between microtubule tips and plasma membrane is reducing after 10 min of Kinesore addition. The effect is enhanced over time.

REFERENCES:

Aher, A., Rai, D., Schaedel, L., Gaillard, J., John, K., Liu, Q., Altelaar, M., Blanchoin, L., Thery, M., & Akhmanova, A. (2020). CLASP Mediates Microtubule Repair by Restricting Lattice Damage and Regulating Tubulin Incorporation. *Current Biology*, *30*(11), 2175–2183. https://doi.org/10.1016/j.cub.2020.03.070

Arellano-Santoyo, H., Geyer, E. A., Stokasimov, E., Chen, G. Y., Su, X., Hancock, W., Rice, L. M., & Pellman, D. (2017). A Tubulin Binding Switch Underlies Kip3/Kinesin-8 Depolymerase Activity. *Developmental Cell*, *42*(1), 37–51.

https://doi.org/10.1016/j.devcel.2017.06.011

Aumeier, C., Schaedel, L., Gaillard, J., John, K., Blanchoin, L., & Théry, M. (2016). Self-repair promotes microtubule rescue. *Nature Cell Biology*, *18*(10), 1054–1064. https://doi.org/10.1038/ncb3406

Block, S., Goldstein, L., & Schnapp, B. (1990). Bead movement by single kinesin molecules studied with optical tweezers. *Nature*, *348*(November), 348–352.

Cai, D., McEwen, D. P., Martens, J. R., Meyhofer, E., & Verhey, K. J. (2009). Single molecule imaging reveals differences in microtubule track selection between kinesin motors. *PLoS Biology*, *7*(10), 1–14. https://doi.org/10.1371/journal.pbio.1000216

Castoldi, M., & Popov, A. V. (2003). Purification of brain tubulin through two cycles of polymerization- depolymerization in a high-molarity buffer. *Protein Expression and Purification*, *32*(1), 83–88. https://doi.org/10.1016/S1046-5928(03)00218-3

Daire, V., Giustiniani, J., Leroy-Gori, I., Quesnoit, M., Drevensek, S., Dimitrov, A., Perez, F., & Poüs, C. (2009). Kinesin-1 regulates microtubule dynamics via a c-Jun N-terminal kinase-dependent mechanism. *Journal of Biological Chemistry*, *284*(46), 31992–32001. https://doi.org/10.1074/jbc.M109.007906

de Forges, H., Pilon, A., Cantaloube, I., Pallandre, A., Haghiri-Gosnet, A. M., Perez, F., & Poüs, C. (2016). Localized Mechanical Stress Promotes Microtubule Rescue. *Current Biology*, *26*(24), 3399–3406. https://doi.org/10.1016/j.cub.2016.10.048

Dimitrov, A., Quesnoit, M., Moutel, S., Cantaloube, I., Poüs, C., & Pérez, F. (2008). Detection of GTP-Tubulin Conformation in Vivo Reveals a Role for GTP Remnants in Microtubule Rescues. *Science*, *322*, 1353–1357.

Dogterom, M., & Leibler, S. (1993). Physical Aspects of the Growth and Regulation of Microtubule Structures. *Physical Review Letters*, *70*(9), 1347–1350.

Drummond, D. R. (2011). Regulation of microtubule dynamics by kinesins. *Seminars in Cell and Developmental Biology*, *22*(9), 927–934. https://doi.org/10.1016/j.semcdb.2011.09.021

Furuta, K., Furuta, A., Toyoshima, Y. Y., Amino, M., Oiwa, K., & Kojima, H. (2013). Measuring collective transport by defined numbers of processive and nonprocessive kinesin motors. *Proceedings of the National Academy of Sciences*, *110*(2), 501–506. https://doi.org/10.1073/pnas.1201390110

Gasic, I., Boswell, S., & Mitchison, T. (2019). Tubulin mRNA stability is sensitive to change in microtubule dynamics caused by multiple physiological and toxic cues. *PLoS Biology*, *17*, 1–23. https://doi.org/10.1101/533224

Hammond, J., Huang, C.-F., Kaech, S., Jacobson, C., Banker, G., & Verhey, K. J. (2010). Posttranslational Modifications of Tubulin and the Polarized Transport of Kinesin-1 in Neurons. *Molecular Biology of the Cell*, *21*, 572–583. https://doi.org/10.1091/mbc.E09

Hancock, W. O., & Howard, J. (1998). Processivity of the motor protein kinesin requires two heads. *Journal of Cell Biology*, *140*(6), 1395–1405. https://doi.org/10.1083/jcb.140.6.1395

Hancock, W. O., & Howard, J. (1999). Kinesin's processivity results from mechanical and

chemical coordination between the ATP hydrolysis cycles of the two motor domains. *Proceedings of the National Academy of Sciences of the United States of America*, *96*(23), 13147–13152. https://doi.org/10.1073/pnas.96.23.13147

Hibbel, A., Bogdanova, A., Mahamdeh, M., Jannasch, A., Storch, M., Schäffer, E., Liakopoulos, D., & Howard, J. (2015). Kinesin Kip2 enhances microtubule growth in vitro through length-dependent feedback on polymerization and catastrophe. *ELife*, *4*(NOVEMBER2015), 1–11. https://doi.org/10.7554/eLife.10542

Hollenbeck, P. J. (1989). The distribution, abundance and subcellular localization of kinesin. *Journal of Cell Biology*, *108*(6), 2335–2342. https://doi.org/10.1083/jcb.108.6.2335

Howard, J., & Hyman, A. A. (2003). Dynamics and mechanics of the microtubule plus end. *Nature*, *422*(6933), 753–758. https://doi.org/10.1038/nature01600

Howard, J., & Hyman, A. A. (2007). Microtubule polymerases and depolymerases. *Current Opinion in Cell Biology*, *19*(1), 31–35. https://doi.org/10.1016/j.ceb.2006.12.009

Hunter, A. W., Caplow, M., Coy, D. L., Hancock, W. O., Diez, S., Wordeman, L., & Howard, J. (2003). The kinesin-related protein MCAK is a microtubule depolymerase that forms an ATP-hydrolyzing complex at microtubule ends. *Molecular Cell*, *11*(2), 445–457. https://doi.org/10.1016/S1097-2765(03)00049-2

Hyman, A. A., Drechsel, D., Kellogg, D., Salser, S., Sawin, K., Steffen, P., Wordeman, L., & Mitchison, T. J. (1991). [39] Preparation of Modified Tubulins. *Methods in Enzymology*, *196*, 478–485.

Jeune-Smith, Y., & Hess, H. (2010). Engineering the length distribution of microtubules polymerized in vitro. *Soft Matter*, *6*(8), 1778–1784. https://doi.org/10.1039/b919488f

Johann, D., Erlenkämper, C., & Kruse, K. (2012). Length regulation of active biopolymers by molecular motors. *Physical Review Letters*, *108*(25), 1–5. https://doi.org/10.1103/PhysRevLett.108.258103

Kaul, N., Soppina, V., & Verhey, K. J. (2014). Effects of α-tubulin K40 acetylation and detyrosination on kinesin-1 motility in a purified system. *Biophysical Journal*, *106*(12), 2636–2643. https://doi.org/10.1016/j.bpj.2014.05.008

Koch, B., Nijmeijer, B., Kueblbeck, M., Cai, Y., Walther, N., & Ellenberg, J. (2018). Generation and validation of homozygous fluorescent knock-in cells using CRISPR-Cas9 genome editing. *Nature Protocols*, *13*(6), 1465–1487. https://doi.org/10.1038/nprot.2018.042

Melbinger, A., Reese, L., & Frey, E. (2012). Microtubule length regulation by molecular motors. *Physical Review Letters*, *108*(25), 1–5. https://doi.org/10.1103/PhysRevLett.108.258104

Melki, R., Fievez, S., & Carlier, M. F. (1996). Continuous monitoring of P(i) release following nucleotide hydrolysis in actin or tubulin assembly using 2-amino-6-mercapto-7-methylpurine ribonucleoside and purine-nucleoside phosphorylase as an enzyme-linked assay. *Biochemistry*, *35*(37), 12038–12045. https://doi.org/10.1021/bi961325o

Mitchison, T., & Kirschner, M. (1984). Microtubule assembly nucleated by isolated centrosomes. *Nature*, *312*(5991), 232–237. https://doi.org/10.1038/312232a0

Muto, E., Sakai, H., & Kaseda, K. (2005). Long-range cooperative binding of kinesin to a

microtubule in the presence of ATP. *Journal of Cell Biology*, *168*(5), 691–696. https://doi.org/10.1083/jcb.200409035

Peet, D. R., Burroughs, N. J., & Cross, R. A. (2018). Kinesin expands and stabilises the GDP-microtubule lattice. *Nature Nanotechnology*, *13*(5), 386–391. https://doi.org/10.1038/s41565-018-0084-4.Kinesin

Provance, D. W., McDowall, A., Marko, M., & Luby-Phelps, K. (1993). Cytoarchitecture of size-excluding compartments in living cells. *Journal of Cell Science*, *106*(2), 565–577.

Randall, T. S., Yip, Y. Y., Wallock-Richards, D. J., Pfisterer, K., Sanger, A., Ficek, W., Steiner, R. A., Beavil, A. J., Parsons, M., & Dodding, M. P. (2017). A small-molecule activator of kinesin-1 drives remodeling of the microtubule network. *Proceedings of the National Academy of Sciences of the United States of America*, *114*(52), 13738–13743. https://doi.org/10.1073/pnas.1715115115

Reid, T. A., Coombes, C., & Gardner, M. K. (2017). Manipulation and quantification of microtubule lattice integrity. *The Company of Biologists*, *6*, 1245–1256. https://doi.org/10.1242/bio.025320

Rogers, K. R., Weiss, S., Crevel, I., Brophy, P. J., Geeves, M., & Cross, R. (2001). KIF1D is a fast non-processive kinesin that demonstrates novel. *Embo Journal*, *20*(18), 5101–5113.

Schaedel, L., John, K., Gaillard, J., Nachury, M. V., Blanchoin, L., & Thery, M. (2015). Microtubules self-repair in response to mechanical stress. *Nature Materials*, *14*(11), 1156–1163. https://doi.org/10.1038/nmat4396

Schaedel, L., Triclin, S., Chrétien, D., Abrieu, A., Aumeier, C., Gaillard, J., Blanchoin, L., Théry, M., & John, K. (2019). Lattice defects induce microtubule self-renewal. *Nature Physics*, *15*, 830–838. https://doi.org/10.1038/s41567-019-0542-4

Shima, T., Morikawa, M., Kaneshiro, J., Kambara, T., Kamimura, S., Yagi, T., Iwamoto, H., Uemura, S., Shigematsu, H., Shirouzu, M., Ichimura, T., Watanabe, T. M., Nitta, R., Okada, Y., & Hirokawa, N. (2018). Kinesin-binding–triggered conformation switching of microtubules contributes to polarized transport. *Journal of Cell Biology*, *217*(12), 4164–4183. https://doi.org/10.1083/jcb.201711178

Soppina, V., Herbstman, J. F., Skiniotis, G., & Verhey, K. J. (2012). Luminal Localization of α-tubulin K40 Acetylation by Cryo-EM Analysis of Fab-Labeled Microtubules. *PLoS ONE*, *7*(10), 1–9. https://doi.org/10.1371/journal.pone.0048204

Triclin, S., Inoue, D., Gaillard, J., Htet, Z. M., Santis, M. De, Portran, D., Derivery, E., Aumeier, C., Schaedel, L., John, K., Leterrier, C., Reck-Peterson, S., Blanchoin, L., & Thery, M. (2018). Self-repair protects microtubules from their destruction by molecular motors. *BioRxiv*, 499020. https://doi.org/10.1101/499020

Vemu, A., Atherton, J., Spector, J. O., Moores, C. A., & Roll-Mecak, A. (2017). Tubulin isoform composition tunes microtubule dynamics. *Molecular Biology of the Cell*, *28*(25), 3564–3572. https://doi.org/10.1091/mbc.E17-02-0124

Vemu, A., Szczesna, E., Zehr, E. A., Spector, J. O., Grigorieff, N., Deaconescu, A. M., & Roll-Mecak, A. (2018). Severing enzymes amplify microtubule arrays through lattice GTP-tubulin incorporation. *Science*, *361*(6404). https://doi.org/10.1126/science.aau1504

Verhey, K. J., Kaul, N., & Soppina, V. (2011). Kinesin Assembly and Movement in Cells.

Annual Review of Biophysics, *40*(1), 267–288. https://doi.org/10.1146/annurev-biophys-042910-155310

Walczak, C. E., Mitchison, T. J., & Desai, A. (1996). XKCM1: A Xenopus kinesin-related protein that regulates microtubule dynamics during mitotic spindle assembly. *Cell*, *84*(1), 37–47. https://doi.org/10.1016/S0092-8674(00)80991-5